

RACER-m Leverages Structural Features for Sparse T Cell Specificity Prediction

Ailun Wang^{1,2}, Xingcheng Lin^{3,4,5,*}, Kevin Ng Chau^{1,2}, José N. Onuchic^{7,8}, Herbert Levine^{1,2,6}, and Jason T. George^{8,9,)**}

¹Center for Theoretical Biological Physics, Northeastern University,
Boston, MA

²Department of Physics, Northeastern University, Boston, MA

³Department of Chemistry, Massachusetts Institute of Technology,
Cambridge, MA

⁴Department of Physics, North Carolina State University, Raleigh, NC

⁵Bioinformatics Research Center, North Carolina State University,
Raleigh, NC

⁶Department of Bioengineering, Northeastern University, Boston, MA

⁷Departments of Physics and Astronomy, Chemistry, and Biosciences,
Rice University, Houston, TX

⁸Center for Theoretical Biological Physics, Rice University, Houston,
TX

⁹Department of Biomedical Engineering, School of Engineering
Medicine, Texas A&M University, Houston, TX

*corresponding author: Xingcheng.Lin@ncsu.edu

**principal corresponding author: jason.george@tamu.edu

August 2023

¹ Abstract

² Reliable prediction of T cell specificity against antigenic signatures is a formidable
³ task, complicated primarily by the immense diversity of T cell receptor and antigen
⁴ sequence space and the resulting limited availability of training sets for inferential
⁵ models. Recent modeling efforts have demonstrated the advantage of incorporating

6 structural information to overcome the need for extensive training sequence data, yet
7 disentangling the heterogeneous TCR-antigen structural interface to accurately pre-
8 dict the MHC-allele-restricted TCR-peptide binding interactions remained challeng-
9 ing. Here, we present RACER-m, a coarse-grained structural template model leverag-
10 ing key biophysical information from the diversity of publicly available TCR-antigen
11 crystal structures. We find explicit inclusion of structural content substantially reduces
12 the required number of training examples for reliable prediction of TCR-recognition
13 specificity and sensitivity across diverse biological contexts. We demonstrate that our
14 structural model capably identifies biophysically meaningful point-mutants that affect
15 overall binding affinity, distinguishing its ability in predicting TCR specificity of point
16 mutants peptides from alternative sequence-based methods. Collectively, our approach
17 combines biophysical and inferential learning-based methods to predict TCR-peptide
18 binding events using sparse training data. Its application is broadly applicable to stud-
19 ies involving both closely-related and structurally diverse TCR-peptide pairs.

20 **1 Introduction**

21 T cell immunity is determined by the interaction of a T cell receptor (TCR) with anti-
22 genic peptide (p) presented on the cell surface via major histocompatibility molecules
23 (MHCs) [1]. T cell activation occurs when there is a favorable TCR-pMHC interac-
24 tion and, for the case of CD8+ effector cells, ultimately results in T cell killing of the
25 pMHC-presenting cell [2]. T cell-mediated antigen recognition confers broad immu-
26 nity against intracellular pathogens as well as tumor-associated antigenic signatures
27 [3]. Thus, a detailed understanding of the specificity of individual T cells in a reper-
28toire comprised of many ($\sim 10^8$) unique T cell clones is required for understanding and
29 accurately predicting many important clinical phenomena, including infection, cancer
30 immunogenicity, and autoimmunity.

31 Due to the immense combinatorial complexity of antigen ($\sim 10^{13}$) and T cell (\sim

32 10^{18}) sequence space, initial conceptual process in the field was made by studying
33 simple forms of amino acid interactions, motivated either by protein folding ideas [4,
34 5] or random energy approaches [6, 7]. Recent advances in high-throughput studies
35 interrogating T cell specificity [8, 9, 10] together with the development of statistical
36 learning approaches have finally enabled data-driven modeling as a tractable approach
37 to this problem. Consequently, a number of approaches have been developed to predict
38 TCR-antigen specificity [11, 12, 13, 14, 15]. A majority of developed approaches
39 input only TCR and pMHC primary sequence information. The persistent challenge
40 with this lies in limited training data given that any reasonable sampling of antigens
41 and T cells, or indeed even an entire human T cell repertoire, represents a very small
42 fraction of sequence space. As a result, many models under-perform on sequences that
43 are moderately dissimilar from their nearest neighbor in the training set, an issue we
44 refer to as *global sparsity*.

45 While global sparsity complicates inference extension to moderately dissimilar
46 antigens, another distinct challenge exists for reliably predicting the behavior of closely
47 related systems that differ by a single amino acid substitution, which we refer to as *lo-*
48 *cal resolvability*. These ‘point-mutated’ systems require predictive methods capable of
49 quantifying the effects of single amino acid changes on the entire TCR-peptide inter-
50 action, a task often limited by lack of sufficient training examples required for reliable
51 estimation of the necessary pairwise residues. Instead, a modeling framework aiming
52 to discern such subtle differences between point-mutants may benefit from learning the
53 general rules of amino acid interactions at the TCR-peptide interface and their varied
54 contributions to binding affinity. Resolving this very particular problem - discerning
55 relevant point-mutations in self-peptide and viral antigens - promises significant ther-
56 apeutic utility in targeting cancer neoantigens, optimally selecting immune stem cell
57 transplant donors, and predicting the immunological consequences of viral variants.
58 Thus local resolvability represents a distinct learning task wherein detailed reliable pre-

59 dictions need to be made on many small variations around a very specific TCR-pMHC
60 system.

61 Several structure-based approaches have also been used to better understand TCR-
62 pMHC specificity. Detailed structural models that focus on a comprehensive descrip-
63 tion of TCR-pMHC interaction, including all-atom simulation and structural relax-
64 ation, are computationally limited to describing a few realized systems of interest
65 [16, 17]. Another strategy develops an AlphaFold-based pipeline to generate accurate
66 3-dimensional structures from primary sequence information to improve the accuracy
67 of TCR-pMHC binding predictions for hundreds of systems [18]. A previous hybrid
68 approach [14] utilized crystal structural data together with known binding sequences to
69 train an optimized binding energy model for describing TCR-pMHC interactions. This
70 approach offered several advantages, including the ability to perform repertoire-level
71 predictions within a reasonable time, along with a reduced demand for extensive train-
72 ing data. However, this model largely focused on a restricted set of peptide or TCR
73 systems using a single MHC-II structural template and did best in explaining mouse
74 I-E^k-restricted systems. Thus, its ability to make reliable predictions for a structurally
75 diverse collection of TCR and peptide pairs with a conserved human leukocyte antigen
76 (HLA) allele restriction remains unknown.

77 Here, we leverage all available protein crystal structures of the most common hu-
78 man MHC-I allele variant - HLA-A*02:01 - to develop a combined sequence-structural
79 model of TCR-pMHC specificity that features biophysical information from a diversity
80 of known structural templates. We quantify the structural diversity in available crystal
81 structures of TCR-pMHC complexes[19, 20, 21], and demonstrate that incorporating a
82 small subset of available structural information is sufficient to enable reliable predic-
83 tions of favorable interactions across a diverse set of TCR-antigen pairs. Our results
84 further suggest that the availability of structural information having close proximity to
85 the true structure of a TCR-pMHC system can ameliorate both global sparsity and local

86 resolvability in discerning the immunogenicity of diverse and point-mutated antigenic
87 variants.

88 **2 Results**

89 **Model development and identification of TCR-peptide pairs with 90 structural templates**

91 We build on our previous RACER framework developed primarily on the mouse MHC-
92 II I-E^k system [14]. Our new approach, termed RACER multi-template (RACER-
93 m), represents a comprehensive pipeline that leverages published crystal structures of
94 known human TCR-pMHC systems. The training data include every available HLA-
95 A*02:01-restricted system with a published structure [PDB/IEDB] of the TCR-pMHC
96 complex along with their corresponding peptide and TCR variable CDR3 α and β se-
97 quences. All associated publications linked to each crystal structure were culled for
98 known strong and weak binding TCR-peptide sequences. Lastly, we included all
99 unique HLA-A*02:01-restricted reads from the ATLAS database [19] comprised of
100 TCR-pMHC systems with reported binding affinity data. In total, 163 unique TCR-
101 peptide pairs and 66 structural templates were identified for training and validation
102 (see Supplementary Data).

103 We next assessed the structural diversity of training templates by pairwise evalua-
104 tion of structural similarity using a previously developed method referred to as mutual
105 Q [22, 23]. Mutual Q similarity defines a structural distance metric consisting of a sum
106 of transformed pairwise distances between each residue in two structures normalized
107 within the range of 0 to 1, which was then used to perform hierarchical clustering. We
108 found that the identified structural clusters largely partition TCR-pMHC systems ac-
109 cording to immunological function (for example, systems sharing a conserved antigen)
110 with a few exceptions (Fig. 2A). Despite our focus only on a specified HLA-restricted

111 repertoire, the analysis nonetheless revealed significant clustering heterogeneity across
112 all included systems: In some cases (e.g. MART-1, TAX), substantial heterogeneity
113 was observed and associated with significant pairwise dissimilarity of TCR and pep-
114 tide sequences. This, together with cross-cluster structural diversity, is a consequence
115 of global sparsity given limited observed structures. On the other hand, we also identi-
116 fied structurally homogeneous clusters comprised of TCR-pMHC systems possessing
117 near-identical pairwise sequence similarity (e.g. 1E6), yet these systems have substan-
118 tial differences in binding affinity, consistent with earlier predictions [6, 7]. This simul-
119 taneous manifestation of global sparsity and local resolvability amongst TCR-peptide
120 systems with identical HLA restriction represents a dual challenge for the development
121 of robust predictive models of TCR-peptide specificity.

122 Given the inter-cluster structural diversity for TCR-pMHC complexes as well as
123 the intra-cluster variability, it is necessary to suitably select a list of structures with
124 sufficient coverage of the identified structural clusters as training data for the model
125 and structural templates for test cases. In particular, we hypothesized that our hybrid
126 structural and sequence-based methodology could benefit from the inclusion of multi-
127 ple template structures, and the modeling approach presented here was developed with
128 this motivation in mind.

129 The flow chart in Fig. 1 illustrates the training (top row) and testing (bottom row)
130 algorithm in RACER-m. For training, contact interactions between peptide and TCR
131 were calculated for each of the strong binding systems with available TCR-pMHC crys-
132 tal structures. Here, contact interactions were defined by a switching function based
133 on the distance between structural residues and a characteristic interaction length (see
134 Methods). For each strong binder, 1000 decoy (weak binder) systems were generated
135 by pairing the original TCR with a randomized version of the peptide. Contact inter-
136 actions derived from the topology of known TCR-pMHC structures, together with a
137 pairwise 20-by-20 symmetric amino acid energy matrix, determine total binding en-

138 ergy. Each value of the energy matrix corresponds to a particular contribution by an
139 amino acid combination, with negative numbers corresponding to attractive contacts.
140 The training objective aims to select the energy matrix that maximizes separability
141 between the binding energy distributions of strong and weak binders.

142 In the testing phase, a sequence threading methods is employed to construct 3D
143 structures for testing cases that lack a solved crystal structure. Here, constructed struc-
144 tures are based on using a chosen known template with shortest (CDR3 α/β and pep-
145 tide) sequence distance to the specific testing case. Using the constructed 3D structure,
146 a contact interface can be similarly calculated for each testing case, and 1000 decoy
147 weak binders can be generated by randomizing the peptide sequence. The optimal en-
148 ergy model is then applied to assign energies to the testing system and decoy binders,
149 and the testing system is identified as a strong binder if its predicted binding energy is
150 significantly lower than the decoy energy distributions based on a standardized z score.
151 Here, z score calculation was adopted from the statistical z-test applied to the predicted
152 binding energy of test systems and decoy weak binders, the latter of which were used
153 as a null distribution to compare against a given test binder. The z score of binding
154 energies is defined as $z = (\bar{E}_{\text{decoy}} - E_{\text{test}})/\sigma_{\text{decoy}}$, where \bar{E}_{decoy} is the average pre-
155 dicted binding energy of decoy weak binders, E_{test} is the predicted binding energy of
156 the testing system, and σ_{decoy} is the standard deviation of the binding energies of de-
157 decoy weak binders. Testing systems having z scores exceeding 1 are considered strong
158 binding.

159 **Structural information enhances recognition specificity of pMHC-
160 TCR complexes**

161 RACER-m was developed to explicitly leverage the available structural information ob-
162 tained from experimentally determined TCR-pMHC complexes for predictions of test-
163 ing cases. While a prior modeling effort [14] relied on a single structural template for

164 both training and testing and achieved reasonable results given reduced training data,
165 structural differences became prominent as the testing data expanded to include addi-
166 tional TCR and peptide diversity, which resulted in reduced predictive utility. Structural
167 variation has been previously observed and quantified in high molecular detail [24, 25]
168 using docking angles [26] and interface parameters.

169 For HLA-A*02:01 TCR-pMHC systems, the docking angles¹ ranged from 29° to
170 73.1°, while the incident angle varied from 0.3° to 39.5° degrees [24, 25, 27]. The
171 observed structural differences among different TCR-pMHC complexes suggest that a
172 single TCR-pMHC complex structure may not accurately represent the contact inter-
173 faces of other TCR-pMHC complexes, particularly those with substantially different
174 docking orientations. These distinct docking orientations lead to large variations in the
175 contact interfaces between peptide and CDR3 α/β loops, which can be observed from
176 the diversity in contact maps as shown in Fig. S1. RACER-m overcomes this limita-
177 tion by the inclusion of 66 TCR-pMHC crystal structures, which are distributed over
178 distinct structural groups, including MART-1, 1E6, TAX, NLV, FLU and serve as both
179 the training dataset and reference template structures for testing cases.

180 In testing TCR-peptide pairs, all corresponding crystal structures were omitted
181 from predictions. Thus, selecting an appropriate template from available structures
182 became crucial for accurately reconstructing the TCR-pMHC interface and estimat-
183 ing the binding energy. To accomplish this, RACER-m assumed that high sequence
184 similarity corresponds to high similarities in the structure space, which is supported
185 by the correlation between mutual Q score and sequence similarity measured from
186 the 66 solved crystal structures of TCR-pMHC complexes (Fig. S2). This assump-
187 tion was implemented by calculating sequence similarity scores of the testing peptide
188 and TCR CDR3 α/β sequences with those of all 66 reference templates. In each case,
189 a position-wise uniform hamming distance on amino acid sequences was calculated

¹The docking angle is the angle between the peptide binding groove on the MHC and the vector between the TCR domains, the latter is calculated using the centroids of the conserved disulfide bonds in each domain. This angle corresponds to the twist of the TCR over the p-MHC.

190 to quantify the similarity. The sum of CDR3 α and β similarities generated the TCR
191 similarity score, and a composite score was created by taking the product of peptide
192 and TCR scores (see Methods). The template structure having the highest sequence
193 similarity was then selected as the template for threading the sequences of the testing
194 TCR-peptide pair.

195 To evaluate the extent to which the RACER-m approach can address global spar-
196 sity by accurately recapitulating observed specificity in the setting of limited training
197 data, we trained a model using 42.3%² of the total experimentally confirmed strong
198 binders, which sparsely cover all the structural groups involved in the mutual Q analy-
199 sis shown in Fig. 2A. The remaining 57.7% of TCR-peptide sequences that lack solved
200 structures were utilized as testing cases to validate the sensitivity of the trained energy
201 model. RACER-m effectively recognizes strong binding peptide-TCR pairs and cor-
202 rectly predicts 98.9% of the testing systems using the criteria that z-score is greater
203 than 1. Amongst the 94 testing systems, only one TCR-peptide pair in the TAX struc-
204 tural group was mis-predicted as a weak binders with a binding energy deviating from
205 the average binding energies of decoy weak binders by 0.64σ , where σ is the standard
206 deviation of the decoy energies. These initial results (Fig. 2) confirm that the model
207 is effectively able to learn the specificity rules from TCR-pMHC systems exhibiting
208 distinct structural representations.

209 While the reliable identification of strong-binding systems is clinically useful and
210 one important measure of model performance, simultaneous evaluation of model speci-
211 ficity is equally crucial for generating useful predictions on the level of a TCR reper-
212toire. To evaluate the specificity of a global sparsity task, we next tested RACER-
213 m's ability to discern experimentally confirmed weak-binding systems. We selected
214 peptides or TCRs from the most abundant structural groups (MART-1 and TAX) in
215 the training set to create 'scrambled' systems by cross-cluster mismatching of either

²In addition to the 66 crystal structures of HLA-A*02:01 TCR-pMHC systems, 3 strong binders (PDB: 3GSR, 3GSU, and 3GSV) of NLV peptide with solved pMHC structures were also included in the training set. See Supporting Methods for details.

216 TCRs or peptides (see Methods for full details). Proceeding in this manner enables
217 a specificity test on biologically realized sequences instead of randomly generated
218 ones. Specifically, every peptide selected from a given structural group (e.g. peptide
219 EAAGIGILTV in the MART-1 group) was mismatched with a list of TCRs specific
220 for peptides belonging to other groups (e.g. TAX, 1E6, FLU, etc.) to form a set of
221 scrambled weak binders.

222 Following our aforementioned testing protocols, we next calculated z-scores for
223 these mismatched interactions, which were then compared to correctly matched sys-
224 tems with the same peptide sequence (e.g. EAAGIGILTV). We also conducted the
225 complementary test on TCRs using scrambled peptides. The primary advantages of
226 this approach include 1) the ability to match amino acid empirical distributions in bind-
227 ing and non-binding pairs, and 2) utilization of realized TCR sequences for specificity
228 assessment instead of random sequences that possess minimal if any overlap with phys-
229 iological sequences.

230 A representative example of these tests utilizing the MART-1 epitope and MART-
231 1-specific TCRs is given in Fig. 3. First, 7 sets of weak binders were constructed by
232 mismatching 36 MART-1-specific TCRs each with 7 non-MART-1 peptides sampled
233 from distinct clusters. We applied RACER-m on each weak binder to predict its bind-
234 ing energy, then compared this value to the distribution of decoy binding energies to
235 obtain a binding z score. z scores of mismatched weak binders, together with those of
236 correctly matched MART-1-TCR strong binders, were used to derive the receiver op-
237 erating characteristic (ROC) curve (Fig. 3A, Fig. S3). The area under the curve (AUC)
238 was greater than or equal to 0.98 for 5 out of 7 test sets, while the others had AUCs of
239 0.80 and 0.75, illustrating RACER-m's ability to successfully distinguish strong bind-
240 ing peptides from mismatched ones in the available MART-1-specific TCR cases.

241 An analogous test was performed on the 5 available peptide variants from the
242 MART-1 structural group by mismatching them with 35 TCR sequences contained

243 in the NLV, FLU, 1E6 or TAX clusters. Relative to the binding energies of correctly
244 matched MART-1-specific TCRs, RACER-m performs well in discerning matched vs
245 mismatched TCRs for 4 out of the 5 tested MART-1 peptides (Fig. 3B, Fig. S4), the
246 one initial exception being peptide ELAGIGILTV. Further inspection of the TCRs in
247 this group revealed that the TAX-specific TCR A6 (triangle sign in Fig. 3C) together
248 with several closely associated point mutants had a z score distribution resembling that
249 of the RD1-MART1High TCR and its associated point mutants (Fig. S4E). This could
250 be explained by the fact that the RD1-MART1High TCR was engineered from the A6
251 TCR to achieve MART-1 specificity [28], wherein A6 was selected because of its simi-
252 larity with MART-1 specific TCRs in the $V\alpha$ region and similar docking mode [28, 29].
253 However, the engineered (RD1-MART1High) TCR is no longer specific to the TAX
254 peptide (LLFGYPVYV), which is consistent with the z scores predicted from RACER-
255 m. Indeed, when the A6-specific TAX peptide is paired with RD1-MART1High TCR,
256 a relatively lower z score (cross sign in Fig. 3C) is predicted in comparison with the z
257 scores from strong binders (violin shape in Fig. 3C) of the same peptide.

258 **Evaluation on extended datasets highlights the added value of struc-
259 tural information**

260 Given RACER-m's performance on the ATLAS data, we then applied the model to
261 additional datasets to further validate its ability in the setting of global sparsity. The 10x
262 genomics [30] dataset details many TCR-peptide binders collected from five healthy
263 donors. HLA-A*02:01-restricted samples in this dataset include 23 unique peptides,
264 and the number of TCRs specific for each peptide varied from 8365 (e.g. GILGFVFTL)
265 to 1 (e.g. ILKEPVHGV). We remark that the diversity of HLA-A*02:01 samples was
266 significantly reduced to 1741 systems having unique CDR3 α/β and peptide sequences
267 after removing redundancies. Importantly, we selected this large dataset as a reasonable
268 test since 89.26% of the 1741 testing systems did not share either the same CDR3 α or

269 CDR3 β sequence in common with the list of available systems used in the training set,
270 and 99.89% of the testing systems did not have the same CDR3 α -CDR3 β combination
271 with the training set, although 7 out of the 23 peptides were shared with the training
272 set.

273 Given this relative lack of overlap with our training data, we applied RACER-m to
274 all unique HLA-A*02:01 pairs. In a majority (88.9%) of these cases across a large im-
275 munological diversity of peptides, RACER-m successfully identifies enriched z scores
276 in the distribution of binding TCRs (Fig. 4A). The distinction of TCRs belonging to
277 testing vs. training sets, together with the striking difference in the size of training and
278 testing systems, suggest that shared structural features were able to augment RACER-
279 m's predictive power on distinct tests. Thus, the inclusion of structural information
280 in model training enhances RACER-m's predictive ability across distinct TCR-pMHC
281 tests. There were several cases where RACER-m's predicted distributions overlapped
282 significantly with low z scores, indicating a failed prediction; in these cases we inves-
283 tigated whether this could be explained by the lack of an appropriate structural tem-
284 plate. A significant positive correlation was observed between a testing case's optimal
285 structural template similarity and the RACER-m-predicted z scores, consistent with a
286 decline in model applicability whenever the closest available template is inadequate for
287 representing the system in question (Fig. S5). Despite this, the RACER-m approach,
288 trained on 69 cases, was able to predict roughly 90% of strong binders contained in
289 over 1700 distinct testing cases in the 10x genomics dataset.

290 We then compared RACER-m's performance to NetTCR-2.0 [11], a well-established
291 convolutional neural network model for predictions of TCR-peptide binding that is
292 trained on over 16000 combinations of peptide/CDR3 α / β sequences. This compari-
293 son was performed on a publicly available list of TCR-pMHC repertoires curated by
294 Zhang *et al.* [12] which were mutually independent of RACER-m or NetTCR-2.0 train-
295 ing data, wherein we included known strong binders and mismatched weak binders for

296 8 unique peptides of HLA-A*02:01. Since NetTCR-2.0 has a restricted length for
297 antigen peptide (no longer than 9-mer), it cannot be applied on testing systems with
298 10-mer peptides such as KLVALGINAV and ELAGIGILTV, which are absent from the
299 NetTCR-2.0 evaluation in Fig. 4B. The area under the ROC curve (AUROC) was used
300 as a standard measure of classification success. In the majority of cases, RACER-
301 m outperformed NetTCR-2.0 in diagnostic accuracy with higher ROC values (Fig.
302 4B). Lastly, RACER-m was further evaluated using an unrelated set of TCR-pMHC
303 data comprised of 400 samples made up of the strong binders and mismatched weak
304 binders with 4 peptides and 100 TCRs [31], which also gives us good distributional
305 performance (Fig. 4C). In one of the 4 peptides included in this dataset, RACER-m
306 seems to have difficulty providing correct classification about strong and weak binders
307 for peptide CVNGSCFTV, which could again be explained by the lack of appropriate
308 structure templates for this pMHC and related strong binding TCRs (Fig. S6).

309 **RACER-m specificity of point-mutated variants and preservation of
310 local resolvability**

311 Encouraged by model handling of global sparsity in tests of disparate binding systems
312 having high sequence diversity, we next evaluated RACER-m's ability in maintaining
313 local resolvability of point-mutated peptides with near-identical sequence similarity to
314 a known strong binder, which represents a distinct and usually more difficult computa-
315 tional problem. Understanding in detail which available point mutants enhance or
316 break immunogenicity is directly relevant for assessing the efficacy of tumor neoanti-
317 gens and T cell responses to viral evolution. Additionally, the performance of structural
318 models in accomplishing this task are a direct readout on their utility over sequence-
319 based methods, since the latter case will struggle to accurately cluster, and therefore
320 resolve, systems having single amino acid differences. To evaluate RACER-m's ability
321 to recognize point mutants, we performed an additional test on an independent compe-

322 hensive dataset of TCR 1E6 containing a point mutagenic screening of the peptide dis-
323 played on MHC. This testing set includes 20 strong binders and 73 weak binders [21],
324 wherein strong binding to the 1E6 TCR was confirmed by $\text{TNF}\alpha$ activity. RACER-m
325 demonstrates enrichment of the distribution of binding energies for strong binders vs.
326 confirmed weak cases (Fig. 5A). ROC analysis of the RACER-m's ability to resolve
327 these groups gives an AUC of 0.78. It is important to note that only 2 strong binders of
328 this system were included in the training of RACER-m's energy model.

329 Inspired by these initial results on the 1E6 mutagenic screen, we extended this
330 analysis to all point-mutated weak binding systems in the ATLAS dataset, specifically
331 those with K_D values greater than $200 \mu\text{M}$. Our results, presented template-wise for
332 each structure in the point-mutant data, demonstrate that RACER-m improves in this
333 recognition task when compared to NetTCR-2.0 (Fig. 5C). Lastly, to explicitly explore
334 the strength of structural modeling in predicting the impact of small but immunologi-
335 cally significant single amino acid differences, we quantified the predicted z scores for
336 both strong and weak binders as a function of sequence similarity (Fig. S7). The re-
337 sults demonstrate that the inclusion of information from correctly identified structural
338 templates enhances RACER-m's predictive power. Collectively, our results suggest
339 that RACER-m offers a unique computational advantage over traditional, sequence-
340 only methods of prediction by leveraging significantly fewer training sequences with
341 key structural information to efficiently identify the contribution of each amino acid
342 change.

343 3 Discussion

344 Reliable and efficient estimation of TCR-pMHC interactions is of central importance
345 in understanding, and thus optimizing, the adaptive immune response. Decoding the
346 predictive rules of TCR-pMHC specificity is a formidable challenge, largely owing to
347 the extreme sparsity of available training data relative to the diversity of sequences that

348 need to be interrogated in meaningful investigation. We developed RACER-m to aug-
349 ment the predictive power of a relatively small number of TCR and epitope sequences
350 by leveraging the structural information contained in solved TCR-pMHC crystal struc-
351 tures. Our analysis focused on the most common human MHC allele variant, due to
352 the abundance of sequence and structural data. Despite this restriction, we observed
353 structural heterogeneity underpinning the specificity of various TCR-pMHC systems
354 in distinct immunological contexts. Enhancement in predictive accuracy was largely
355 driven by the availability of a small list of structural templates, which included 66
356 crystal structures of TCR-pMHC complexes from the Protein Data Bank.

357 Using our minimal list, together with mutually independent testing systems for
358 RACER-m and NetTCR-2.0, we find that our model is able to outperform on both
359 detection of strong binders as well as avoidance of weak binders - both representing
360 distinct but equally important tasks. We advocate for the inclusion of such mixed
361 performative tests for rigorous validation as a necessary and standardized component
362 in model evaluation, in addition to model comparisons using testing data that is equally
363 dissimilar from the training data included in competing models.

364 Intriguingly, incorporation of structural information into the training approach en-
365 ables the development of a model that maintains predictive accuracy while dealing with
366 both global sparsity and local resolvability, all while requiring substantially reduced
367 training sequence data. Our results suggest that a wealth of information is contained in
368 the structural templates pertaining to key contributors of a favorable TCR-peptide inter-
369 action, wherein conserved features across distinct systems can be learned to mitigate
370 global sparsity. Conversely, structural encoding of information pertinent to residues
371 whose amino acid substitutions either preserve or break immunogenicity also assists
372 RACER-m trained on only a small subset of all possible point-mutagens by identifying
373 key contributing positions and residues, thereby preserving local resolvability.

374 Moreover, model accuracy correlated directly with the availability of a template

375 having sufficient proximity to the sequences of testing systems. As a result, we an-
376 ticipate that RACER-m will improve as more structures become readily available for
377 inclusion. Existing computational methods for identifying structural models from pri-
378 mary sequence data [18] may provide an efficient method of adding highly informa-
379 tive structures into the candidate pool for testing. This, together with identifying the
380 minimal sufficient number of distinct structural classes within a given MHC allele re-
381 striction remain tasks for subsequent investigation. Our current results suggest this is
382 doable given the small number of structures available for explaining the diverse systems
383 studied herein. Significantly, the inclusion of only 66 template structure augmented
384 RACER-m's ability to accurately differentiate strong and weak binders when eval-
385 uated with hundreds and even thousands of testing systems. This structural advantage
386 was enhanced both by the approach of hybridizing sequence and structural information
387 into the training and testing protocols and the availability of templates that shared suffi-
388 cient sequence-based similarity to testing cases so that an adequate threading template
389 was available.

390 4 Methods

391 RACER-m Model.

392 To predict the binding affinity between a given TCR-peptide pair, we employed a
393 pairwise energy model to assess the TCR-peptide binding energy [14]. The CDR3 α
394 & CDR3 β regions were used to differentiate between different TCRs because CDR3
395 loops primarily interact with the antigen peptides while CDR1 and CDR2 interact with
396 MHC [32]. However, the binding energy was evaluated based on the entire binding
397 interface between TCR and peptide. As illustrated in Fig. 1, we included 66 experi-
398 mentally determined TCR-p-MHC complex structures and 3 additional TCR-p-MHC
399 complex structures composed of experimentally determined p-MHC complexes with

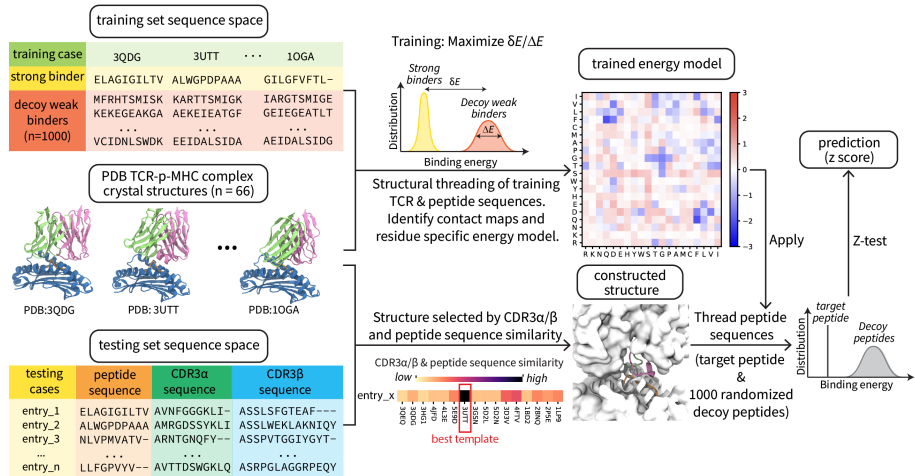


Figure 1: Model architecture of RACER-m. Schematic representation of the training (top row) and testing (bottom row) processes in RACER-m. 66 Crystal structures of known strong binders were used as both training set and template structures for the testing processes, which covers several major clusters of TCR repertoires (MART-1, TAX, 1E6, NLV, FLU) and other clusters with smaller size.

400 corresponding TCR structures as strong binders for training an energy model (details
 401 in Supporting Methods), which was subsequently used to evaluate binding energies of
 402 other TCR-peptide pairs based on their CDR3 and peptide sequences. Additionally,
 403 for each strong binder, we generated 1000 decoys by randomizing the peptide
 404 sequence. These 69,000 decoys constitute an ensemble of weak binders within our
 405 training set.

406 To parameterize this energy model, we optimized the parameters by maximizing the
 407 gap of binding energies between the strong and weak TCR-peptide binders, represented
 408 by δE in Fig. 1. The resulting optimized energy model will be used for predicting the
 409 binding specificity of a peptide towards a given TCR based on their sequences. Further
 410 details regarding the calculation of binding energy are provided below.

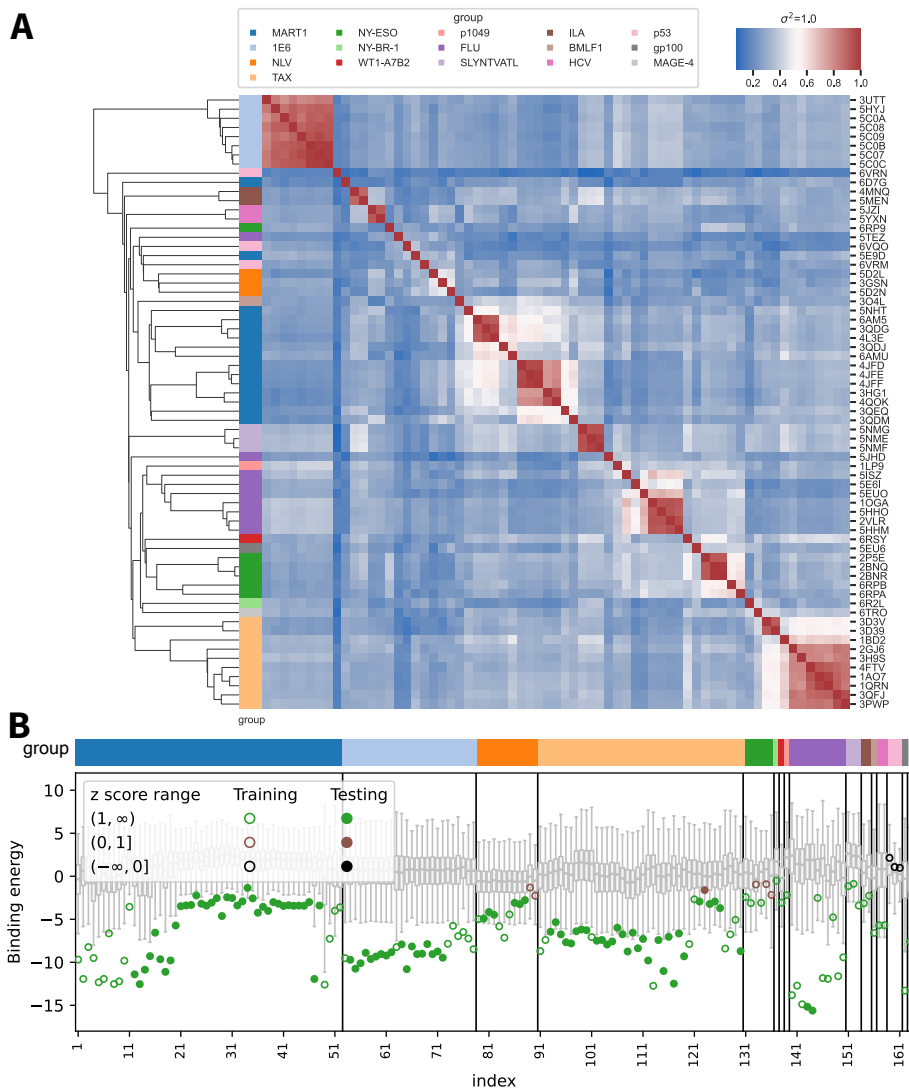


Figure 2: Performance on ATLAS dataset (A) Mutual Q calculation results between all crystal structures in training set of RACER-m, which measures the structural similarity between every pair of structures from the training set. The linkage map shows the hierarchical clustering result based on the pairwise mutual Q values. Color blocks next to the linkage map indicates the corresponding cluster of the crystal structure in the row. (B) Predicted binding energies for ATLAS dataset (open circles and closed dots) in comparison with the binding energies for corresponding weak binders (box plots). Each open circle represents the predicted binding energy for a structure in the training set, while each closed dot represents the predicted binding energy for a testing case from ATLAS dataset. Each training or testing case is associated with 1000 decoy weak binders generated by randomizing the peptide sequence and pairing with the TCR in the corresponding training/testing structure. Box plots represents the distribution of the predicted energies of the decoy weak binders with the box representing the lower (Q1) to upper (Q3) quartiles and a horizontal line representing the median. The whiskers extended from the box by 1.5IQR, where IQR indicates the interquartile range.

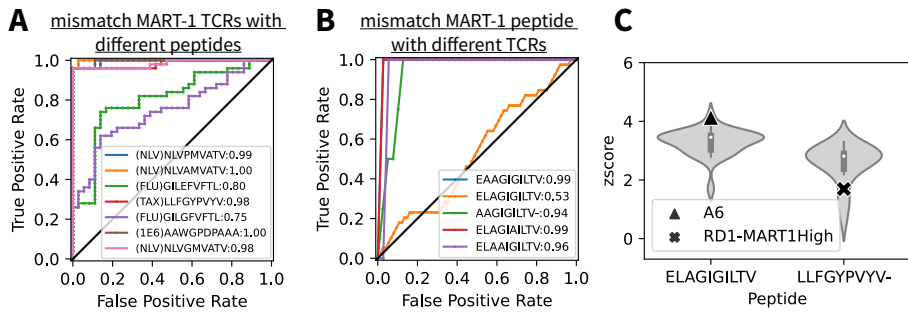


Figure 3: Prediction performance on weak binders generated by mismatching peptides with TCRs. (A) ROC curves for RACER-m classification performance on differentiating weak binders generated by mismatching peptides from NLV, TAX, FLU and 1E6 clusters with MART-1 TCRs from MART-1 strong binders with the same set of TCRs. (B) ROC curves for RACER-m classification performance on distinguishing MART-1 strong binders from mismatched weak binders generated by pairing MART-1 specific peptides with TCRs from NLV, TAX, FLU and 1E6 clusters. (C) When TAX A6 TCR is paired with MART-1 peptide ELAGIGILTV, the Z-score of the mismatched system (triangle) resembles the values from the strong binders (violin shape) formed by the same peptide and TCR RD1-MART1High and its point mutants, which was engineered from A6. In the reverse scenario, TCR RD1-MART1High shows lower Z-score (cross) than TAX strong binders (violin shape) when paired with TAX specific peptide LLFVYPVYV.

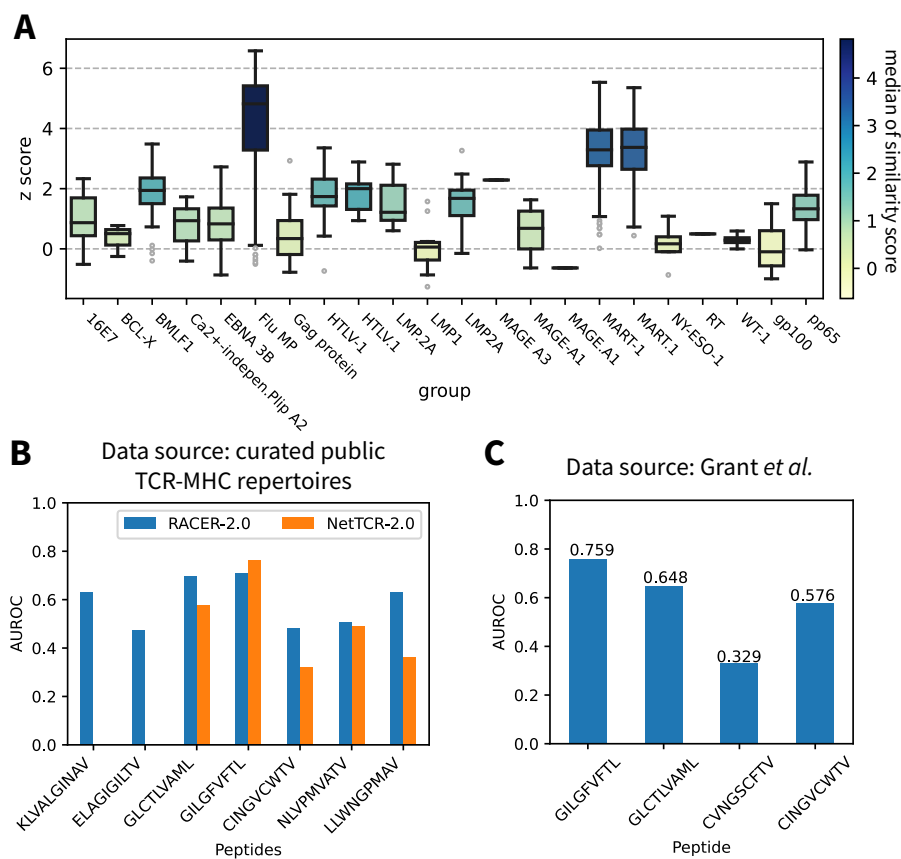


Figure 4: Validate the predictive power of RACER-m with external datasets. (A) Prediction results of RACER-m on the HLA-A*02:01 restricted systems from 10x Genomics dataset collected from 5 healthy donors. 1741 unique pairs of TCR-peptide sequences were tested and the prediction results of z score were grouped by the immunological profile of the test systems and depicted as box plots. (B) Comparison of classification performance between RACER-m and NetTCR-2.0 on a curated list of public TCR-pMHC repertoires [12] comprised by both strong binders and mismatched weak binder. Due to the restriction of NetTCR-2.0 on the peptide length (9-mer), there is no data from NetTCR-2.0 for the two 10-mer peptides (KLVALGINAV and ELAGIGILTV). (C) The classification performance of RACER-m on another set of TCR-pMHC test systems [31].

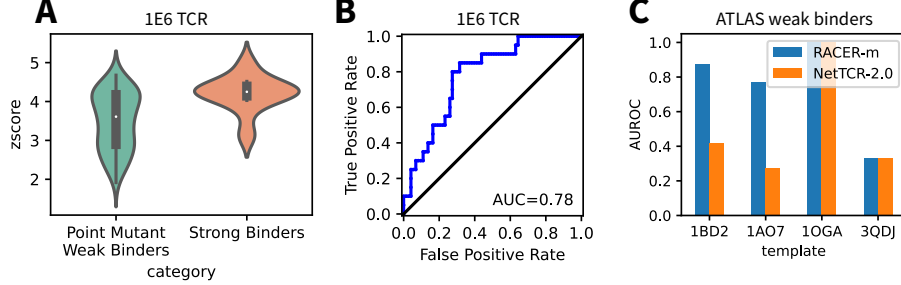


Figure 5: **RACER-m's performance on differentiating strong binders from point-mutant weak binders** (A) Distribution of z scores from strong binders of 1E6 TCR and weak binders from point mutagenic screen. (B) ROC curve for RACER-m classification performance using the strong and point-mutant weak binders for 1E6 TCR. (C) Comparison of RACER-m and NetTCR-2.0 in classification of strong and point-mutant weak binders from ATLAS dataset.

411 **Detailed calculation of TCR-peptide binding energies**

412 To evaluate the binding affinity between a TCR and a peptide, RACER-m utilized
 413 the framework of the AWSEM force field [33], which is a residue-resolution protein
 414 force field widely used for studying protein folding and binding [33, 34]. To adapt the
 415 AWSEM force field for predicting TCR-peptide binding energy, we utilized its direct
 416 protein-protein interaction component to calculate the inter-residue contacting interac-
 417 tions at the TCR-peptide interface. Specifically, we utilized the $C\beta$ atoms (except for
 418 glycine, where $C\alpha$ atom was used instead) of each residue to calculate the contacting
 419 energy using the following expression:

$$V_{direct} = \sum_{i \in \text{TCR}, j \in \text{peptide}} \gamma_{i,j}(a_i, a_j) \Theta_{i,j}^I \quad (1)$$

420 In Eq. 1, $\Theta_{i,j}$ represents a switching function that defines the effective range of inter-
 421 actions between each amino acid from the peptide and the TCR:

$$\Theta_{i,j}^I = \frac{1}{4} (1 + \tanh[5.0 \times (r_{i,j} - r_{\min}^I)]) (1 + \tanh[5.0 \times (r_{\max}^I - r_{i,j})]) \quad (2)$$

422 where $r_{\min}^I = 6.5\text{\AA}$ and $r_{\max}^I = 8.5\text{\AA}$. The coefficients $\gamma_{i,j}(a_i, a_j)$ define the strength
423 of interactions based on the types of amino acids (a_i, a_j). The $\gamma_{i,j}(a_i, a_j)$ coefficients
424 are also the parameters that are trained in the optimization protocols described as fol-
425 lows.

426 **Optimization of energy model for predicting the TCR-peptide bind-
427 ing specificity.**

428 To predict the binding specificity between a given TCR and peptide, the energy model
429 is trained using interactions gathered from the known strong binders and their corre-
430 sponding randomly generated decoy binders. Following the protocol specified in our
431 previous paper [14], the energy model of RACER-m was trained to maximize the gap
432 between the binding energies of strong and weak binders. In addition, a larger training
433 set was used to achieve a more comprehensive coverage of the structural and sequence
434 space. Specifically, the binding energies were calculated from individual strong binders
435 (E_{strong}) and their corresponding decoy weak binders (E_{decoy}) as described in Eq. 1.
436 We then calculated the average binding energy of the strong ($\langle E_{\text{strong}} \rangle$), the average
437 binding energy of the decoy weak binders ($\langle E_{\text{decoy}} \rangle$), and the standard deviation of the
438 energies of the decoy weak binders (ΔE).

439 To train the model, the parameters $\gamma_{i,j}(a_i, a_j)$ were optimized to maximize $\delta E / \Delta E$,
440 where $\delta E = \langle E_{\text{decoy}} \rangle - \langle E_{\text{strong}} \rangle$, resulting in the maximal separation between strong
441 and weak binders. Mathematically, δE can be represented as $\mathbf{A}^T \gamma$, where

$$\mathbf{A} = \langle \phi_{\text{decoy}} \rangle - \langle \phi_{\text{strong}} \rangle. \quad (3)$$

442 Furthermore, the standard deviation of the decoy binding energies ΔE can be calcu-
443 lated as $\Delta E^2 = \gamma^T B \gamma$, where

$$B = \langle \phi_{\text{decoy}} \phi_{\text{decoy}}^T \rangle - \langle \phi_{\text{decoy}} \rangle \langle \phi_{\text{decoy}} \rangle^T, \quad (4)$$

444 here, ϕ takes the functional form of V_{direct} and summarizes interactions between differ-
445 ent types of amino acids. Therefore, the vector \mathbf{A} specifies the difference in interaction
446 strengths for each pair of amino acid types between the strong and decoy binders, with
447 a dimension of (1,210), while the matrix B is a covariance matrix with a dimension of
448 (210, 210).

449 With the definition above, maximizing the objective function of $\delta E/\Delta E$ can be
450 reformulated as maximization of $\mathbf{A}^\top \gamma / \sqrt{\gamma^\top B \gamma}$. This maximization can be effectively
451 achieved through maximizing the functional objective $R(\gamma) = \mathbf{A}^\top \gamma - \lambda_1 \sqrt{\gamma^\top B \gamma}$. By
452 setting $\partial R(\gamma)/\partial \gamma^\top$ to 0, the optimization process leads to $\gamma \propto B^{-1} \mathbf{A}$, where γ is a
453 (210, 1) vector encoding the trained strength of each type of amino acid-amino acid
454 interactions. For visualization purposes, the vector γ is reshaped into a symmetric 20-
455 by-20 matrix, as shown in Fig.1. Additionally, a filter is applied to reduce the noise
456 caused by the finite sampling of decoy binders. In this filter, the first 50 eigenvalues
457 of the B matrix are retained, and the remaining eigenvalues are replaced with the 50th
458 eigenvalue.

459 **Construction of target TCR-p-MHC complex structures from se-
460 quences.**

461 Since RACER-m calculates the binding energy based on the interaction contacts be-
462 tween a given peptide and a TCR, it relies on the 3D structure of the TCR-p-MHC
463 complex for contact calculation. Although the training data include a 3D structure for
464 each of the TCR-peptide strong binders, we usually lack 3D structures for most of the
465 testing cases. To address this limitation, we used the software Modeller [35] to con-
466 struct a structure based on the target peptide/CDR3 sequences in the test system and a
467 template crystal structure selected from the training set.

468 Specifically, for each testing system, a position-wise uniform Hamming distance
469 was computed between the target sequence and each of the sequences from the 66

470 training strong binders with complete TCR-p-MHC complex structures, separately for
471 peptide, CDR3 α , and CDR3 β regions. Then, sequence similarity scores were assigned
472 to peptide, CDR3 α , and CDR3 β , respectively with the number of amino acids that
473 remain the same between target and template sequences. To calculate a composite
474 similarity score for the target TCR-peptide complex, we summed the similarity scores
475 of the CDR3 α and β regions and multiplied this sum by the peptide similarity score.
476 The template structure with the highest similarity score was selected as the template
477 for the subsequent sequence replacement using Modeller (Fig. 1 bottom).

478 To perform the sequence replacement, the peptide, CDR3 α , and CDR3 β sequences
479 in the template structure were replaced with the corresponding target sequences in the
480 testing TCR-peptide system. The location of the target sequence in the template struc-
481 ture was determined by aligning the first amino acid of the target sequence with the
482 original template sequence. If the two sequences had different lengths, the remaining
483 locations were patched with gaps. This sequence alignment and the selected template
484 structure were then used as input for Modeller to generate a new structure. The con-
485 structed structure was then used for the estimation of the binding energy of the testing
486 system.

487 **Generation of weak binders by mismatching sequences of known
488 TCR-peptide pairs**

489 To test the performance of RACER-m in distinguishing strongly bound TCR-peptide
490 pairs from weak binders, we generated a set of weak binders by introducing sequence
491 mismatches between the peptides and TCRs from the known strongly bound TCR-
492 peptide pairs. As shown in Fig. 2, the strong binders were grouped based on their
493 immunological systems, such as MART-1 and TAX. It is important to note that pairs
494 within the same group also share similar TCR-peptide structural interfaces.

495 To generate the weak binders, we mismatched the sequences of peptides and the

496 CDR3 α/β pairs from different groups. For example, 36 pairs of MART-1 specific
497 CDR3 α/β sequences were mismatched with 7 non-MART-1 peptides to form weak
498 binders for Fig. 3A, while 5 MART-1 specific peptides were mismatched with 35
499 pairs of non-MART-1 CDR3 α/β sequences to form weak binders in Fig. 3B. The
500 newly generated combinations of sequences were then used to create 3D structures of
501 the TCR-p-MHC complexes, following the protocol specified in Section *Constructing*
502 *TCR-p-MHC complex structure from sequence.*

503 **Mutual Q calculation.**

504 To quantify the structural distances between the 66 crystal structures of TCR-p-MHC
505 complexes, a pairwise mutual Q score was used to calculate the structural similarity
506 between every pair of the 66 structures. Since our focus is on the contact interface be-
507 tween the peptide and the CDR3 $\alpha/CDR3\beta$ loops of the TCR, the mutual Q score was
508 computed between these regions. We adopted a similar protocol used in [22] and cal-
509 culated the mutual Q score between structures A and B with the following expression:

$$Q^{A,B} = c \sum_{i \in \text{peptide}, j \in \text{CDR3}} \exp \left[-\frac{(r_{ij}^A - r_{ij}^B)^2}{2\sigma^2} \right] \quad (5)$$

510 where i and j are indices of atoms from the peptide and CDR3 loops, respectively.
511 r_{ij}^A and r_{ij}^B denote the contact distances between atom i and j in structure A and B
512 respectively. For simplicity, σ was set as 1 Å instead of using the sequence distance
513 between i and j as done in [22]. The coefficient c normalizes the value of Q to fall
514 within the range of 0 and 1. This definition ensures that a larger value of Q indicates a
515 greater structural similarity between the two systems.

516 **Prediction protocols with NetTCR-2.0.**

517 To test the predictive performance of RACER-m, we compared the prediction accuracy
518 of RACER-m with NetTCR-2.0, another widely used computational tool trained with
519 a convolutional neural network model, as described by Montemurro *et al.* [11]. To en-
520 sure a fair comparison, we retrained the NetTCR-2.0 model with the paired alpha beta
521 dataset with a 95% partitioning threshold (file train_ab_95_alpha_beta.csv, provided in
522 <https://github.com/mnieldLab/NetTCR-2.0>). The trained model was then used to clas-
523 sify the strong and weak binders, as shown in Fig. 5C. Due to the peptide length re-
524 striction in the application of NetTCR-2.0, we excluded peptides longer than 9 residues
525 from our testing prediction.

526 **Acknowledgments**

527 Work by the Center for Theoretical Biological Physics was supported by the NSF
528 (Grant PHY-2019745). JTG was supported by CPRIT grant RR210080. JNO was
529 also supported by the NSF grant PHY-2210291 and by the Welch Foundation (Grant
530 C-1792). JNO and JTG are CPRIT Scholars in Cancer Research.

531 **References**

532 [1] Ludger Klein, Bruno Kyewski, Paul M Allen, and Kristin A Hogquist. Positive
533 and negative selection of the t cell repertoire: what thymocytes see (and don't
534 see). *Nature Reviews Immunology*, 14(6):377–391, 2014.

535 [2] Arash Grakoui, Shannon K Bromley, Cenk Sumen, Mark M Davis, Andrey S
536 Shaw, Paul M Allen, and Michael L Dustin. The immunological synapse: a
537 molecular machine controlling t cell activation. *Science*, 285(5425):221–227,
538 1999.

539 [3] Sadia Ilyas and James C Yang. Landscape of tumor antigens in t cell immunotherapy. *The Journal of Immunology*, 195(11):5117–5122, 2015.

540

541 [4] Andrej Košmrlj, Abhishek K Jha, Eric S Huseby, Mehran Kardar, and Arup K Chakraborty. How the thymus designs antigen-specific and self-tolerant t cell receptor sequences. *Proceedings of the National Academy of Sciences*, 105(43):16671–16676, 2008.

542

543

544

545 [5] Arup K Chakraborty and Andrej Košmrlj. Statistical mechanical concepts in immunology. *Annual review of physical chemistry*, 61:283–303, 2010.

546

547 [6] Jason T George, David A Kessler, and Herbert Levine. Effects of thymic selection on t cell recognition of foreign and tumor antigenic peptides. *Proceedings of the National Academy of Sciences*, 114(38):E7875–E7881, 2017.

548

549

550 [7] Kevin Ng Chau, Jason T George, José N Onuchic, Xingcheng Lin, and Herbert Levine. Contact map dependence of a t-cell receptor binding repertoire. *Physical Review E*, 106(1):014406, 2022.

551

552

553 [8] Michael E Birnbaum, Juan L Mendoza, Dhruv K Sethi, Shen Dong, Jacob Glanville, Jessica Dobbins, Engin Özkan, Mark M Davis, Kai W Wucherpfennig, and K Christopher Garcia. Deconstructing the peptide-mhc specificity of t cell recognition. *Cell*, 157(5):1073–1087, 2014.

554

555

556

557 [9] Pradyot Dash, Andrew J Fiore-Gartland, Tomer Hertz, George C Wang, Shalini Sharma, Aisha Souquette, Jeremy Chase Crawford, E Bridie Clemens, Thi HO Nguyen, Katherine Kedzierska, et al. Quantifiable predictive features define epitope-specific t cell receptor repertoires. *Nature*, 547(7661):89–93, 2017.

558

559

560

561 [10] Stephane C Boutet, Dagmar Walter, Michael JT Stubbington, Katherine A Pfeifer, Josephine Y Lee, Sarah EB Taylor, Luz Montesclaros, Julia K Lau, Daniel P

562

563 Riordan, Alvaro Martinez Barrio, et al. Scalable and comprehensive characteri-
564 zation of antigen-specific cd8 t cells using multi-omics single cell analysis. The
565 Journal of Immunology, 202(1_Supplement):131–4, 2019.

566 [11] Alessandro Montemurro, Viktoria Schuster, Helle Rus Povlsen, Amalie Kai
567 Bentzen, Vanessa Jurtz, William D Chronister, Austin Crinklaw, Sine R Hadrup,
568 Ole Winther, Bjoern Peters, et al. Nettcr-2.0 enables accurate prediction of tcr-
569 peptide binding by using paired tcr α and β sequence data. Communications
570 biology, 4(1):1060, 2021.

571 [12] Wen Zhang, Peter G Hawkins, Jing He, Namita T Gupta, Jinrui Liu, Gabrielle
572 Choonoo, Se W Jeong, Calvin R Chen, Ankur Dhanik, Myles Dillon, et al. A
573 framework for highly multiplexed dextramer mapping and prediction of t cell re-
574 ceptor sequences to antigen specificity. Science Advances, 7(20):eabf5835, 2021.

575 [13] John-William Sidhom, H Benjamin Larman, Drew M Pardoll, and Alexander S
576 Baras. Deeptcr is a deep learning framework for revealing sequence concepts
577 within t-cell repertoires. Nature communications, 12(1):1605, 2021.

578 [14] Xingcheng Lin, Jason T George, Nicholas P Schafer, Kevin Ng Chau, Michael E
579 Birnbaum, Cecilia Clementi, José N Onuchic, and Herbert Levine. Rapid assess-
580 ment of t-cell receptor specificity of the immune repertoire. Nature computational
581 science, 1(5):362–373, 2021.

582 [15] Ido Springer, Nili Tickotsky, and Yoram Louzoun. Contribution of t cell receptor
583 alpha and beta cdr3, mhc typing, v and j genes to peptide binding prediction.
584 Frontiers in immunology, 12:664514, 2021.

585 [16] Brian G Pierce, Lance M Hellman, Moushumi Hossain, Nishant K Singh,
586 Craig W Vander Kooi, Zhiping Weng, and Brian M Baker. Computational design
587 of the affinity and specificity of a therapeutic t cell receptor. PLoS computational
588 biology, 10(2):e1003478, 2014.

589 [17] Chen Yanover and Philip Bradley. Large-scale characterization of peptide-mhc
590 binding landscapes with structural simulations. Proceedings of the National
591 Academy of Sciences, 108(17):6981–6986, 2011.

592 [18] Philip Bradley. Structure-based prediction of t cell receptor: peptide-mhc inter-
593 actions. eLife, 12:e82813, 2023.

594 [19] Tyler Borrman, Jennifer Cimons, Michael Cosiano, Michael Purcaro, Brian G
595 Pierce, Brian M Baker, and Zhiping Weng. Atlas: a database linking binding
596 affinities with structures for wild-type and mutant tcr-pmhc complexes. Proteins:
597 Structure, Function, and Bioinformatics, 85(5):908–916, 2017.

598 [20] Christopher Szeto, Christian A Lobos, Andrea T Nguyen, and Stephanie Gras.
599 Tcr recognition of peptide–mhc-i: rule makers and breakers. International journal
600 of molecular sciences, 22(1):68, 2020.

601 [21] Anna M Bulek, David K Cole, Ania Skowera, Garry Dolton, Stephanie Gras,
602 Florian Madura, Anna Fuller, John J Miles, Emma Gostick, David A Price, et al.
603 Structural basis for the killing of human beta cells by cd8+ t cells in type 1 dia-
604 betes. Nature immunology, 13(3):283–289, 2012.

605 [22] Mingchen Chen, Xingcheng Lin, Wei Lu, José N Onuchic, and Peter G Wolynes.
606 Protein folding and structure prediction from the ground up ii: Aawsem for α/β
607 proteins. The journal of physical chemistry B, 121(15):3473–3482, 2017.

608 [23] Samuel S Cho, Yaakov Levy, and Peter G Wolynes. P versus q: Structural reaction
609 coordinates capture protein folding on smooth landscapes. Proceedings of the
610 National Academy of Sciences, 103(3):586–591, 2006.

611 [24] Ragul Gowthaman and Brian G Pierce. Tcr3d: The t cell receptor structural
612 repertoire database. Bioinformatics, 35(24):5323–5325, 2019.

613 [25] Ragul Gowthaman and Brian G Pierce. Modeling and viewing t cell receptors
614 using tcrmodel and tcr3d. *Bioinformatics for Cancer Immunotherapy: Methods*
615 and *Protocols*, pages 197–212, 2020.

616 [26] Markus G Rudolph, Robyn L Stanfield, and Ian A Wilson. How tcrs bind mhcs,
617 peptides, and coreceptors. *Annu. Rev. Immunol.*, 24:419–466, 2006.

618 [27] Brian G Pierce and Zhiping Weng. A flexible docking approach for prediction of
619 t cell receptor–peptide–mhc complexes. *Protein Science*, 22(1):35–46, 2013.

620 [28] Sheena N Smith, Yuhang Wang, Javier L Baylon, Nishant K Singh, Brian M
621 Baker, Emad Tajkhorshid, and David M Kranz. Changing the peptide speci-
622 ficity of a human t-cell receptor by directed evolution. *Nature communications*,
623 5(1):5223, 2014.

624 [29] Brian G Pierce, Lance M Hellman, Moushumi Hossain, Nishant K Singh,
625 Craig W Vander Kooi, Zhiping Weng, and Brian M Baker. Computational design
626 of the affinity and specificity of a therapeutic t cell receptor. *PLoS computational*
627 *biology*, 10(2):e1003478, 2014.

628 [30] 10x Genomics. A new way of exploring immunity–linking highly multiplexed
629 antigen recognition to immune repertoire and phenotype. *Tech. rep.*, 2019.

630 [31] Emma J Grant, Tracy M Josephs, Sophie A Valkenburg, Linda Wooldridge, Mar-
631 garet Hellard, Jamie Rossjohn, Mandvi Bharadwaj, Katherine Kedzierska, and
632 Stephanie Gras. Lack of heterologous cross-reactivity toward hla-a* 02: 01
633 restricted viral epitopes is underpinned by distinct $\alpha\beta$ t cell receptor signatures.
634 *Journal of Biological Chemistry*, 291(47):24335–24351, 2016.

635 [32] Nicole L La Gruta, Stephanie Gras, Stephen R Daley, Paul G Thomas, and Jamie
636 Rossjohn. Understanding the drivers of mhc restriction of t cell receptors. *Nature*
637 *Reviews Immunology*, 18(7):467–478, 2018.

638 [33] Aram Davtyan, Nicholas P Schafer, Weihua Zheng, Cecilia Clementi, Peter G
639 Wolynes, and Garegin A Papoian. Awsem-md: Protein structure prediction us-
640 ing coarse-grained physical potentials and bioinformatically based local structure
641 biasing. *The Journal of Physical Chemistry B*, 116(29):8494–8503, 2012.

642 [34] Weihua Zheng, Nicholas P Schafer, Aram Davtyan, Garegin A Papoian, and Pe-
643 ter G Wolynes. Predictive energy landscapes for protein–protein association.
644 *Proceedings of the National Academy of Sciences*, 109(47):19244–19249, 2012.

645 [35] Benjamin Webb and Andrej Sali. Comparative protein structure modeling using
646 modeller. *Current protocols in bioinformatics*, 54(1):5–6, 2016.